stellarator news

Published by Fusion Energy Division, Oak Ridge National Laboratory
Building 5700 P.O. Box 2008 Oak Ridge, TN 37831-6169, USA

Editor: James A. Rome Issue 109 June 2007
E-Mail: jar@ornl.gov Phone (865) 482-5643
On the Web at *http://www.ornl.gov/sci/fed/stelnews*

On the damping of edge radial electric fields and flows in the TJ-II stellarator

Plasma flows play crucial roles in magnetically confined fusion plasmas [1–3]. Both neoclassical (e.g., ion orbit losses [4]) and anomalous mechanisms (i.e., anomalous stringer spin-up [5], Reynolds stress [6, 7]) have been considered as candidates to explain the generation of sheared flows.

Electrode biasing experiments were carried out in TJ-II to study the generation of radial electric fields and the driving and damping mechanisms involved. Measurements have been taken in electron cyclotron resonance heated (ECRH) plasmas (P_{ECRH}= 200–400 kW, B_T = 1 T, R = 1.5 m, $\langle a \rangle$ = 0.22 m, $\iota(a) \approx 1.7$–1.8) with densities in the range (0.35–1.0) × 10^{19} m^{-3}. A carbon composite mushroom-shaped electrode (12 mm high, 25 mm diameter) was used to externally modify the electric field. The electrode was inserted typically 2 cm (up to $r/a \approx 0.9$) inside the last closed flux surface (LCFS) and, for the present experiments, was biased positively (200–300 V) with respect to one of the two TJ-II limiters located in the scrape-off layer region (about 0.5 cm beyond the LCFS). Measured electrode currents were in the range of 30–50 A [8]. Different edge plasma parameters were characterized using a multi-Langmuir probe system installed on a fast reciprocating probe drive.

The effects of electrode bias in TJ-II on both global (plasma density increased >20% plus decrease of H_α radiation) and local (reduction of turbulent transport and fluctuation levels) plasma parameters are consistent with an improvement in plasma confinement. The modifications in the plasma properties induced by electrode biasing depend on several parameters, such as the biasing voltage, the electrode location, and the plasma density [8]. Previous experiments in TJ-II have shown that the development of the naturally occurring velocity shear layer requires a minimum plasma density (and/or gradient) [9]. In the region just inside the LCFS, the radial electric field increases significantly when the plasma density reaches this threshold value. The response of the plasma to bias is therefore different for densities below and above the threshold value needed to trigger the spontaneous development of **E**×**B** sheared flows. The results presented correspond to positive applied biasing and different plasma density values below and above the density threshold.

In this issue . . .

The floating potential profile is strongly modified by the electrode bias in the region $r/a < 0.9$, leading to the formation of a strong positive radial electric field (up to 10 kV/m); consequently the perpendicular phase velocity changes sign during biasing. Ion saturation current profiles (i.e., edge electron density) become steeper during biasing in the region where the electric field is modified.

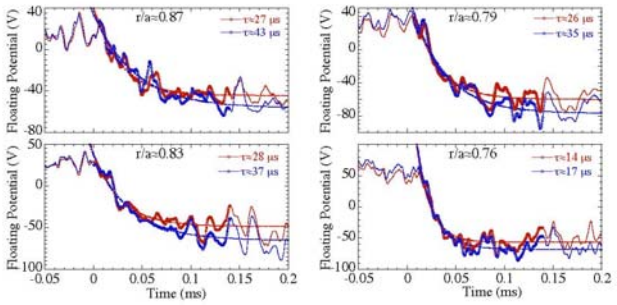

Fig. 1. Two simultaneously measured floating potentials signals and decay fitting function for different radial probe positions in TJ-II. Biasing was switched off at Time = 0.

Two different time scales have been observed in the decay of the edge plasma potential when electrode biasing is switched off. The first is a slow time scale of the order of tens of milliseconds (comparable to the particle confinement time) that is directly linked to the evolution of plasma density. Second, strong changes in the plasma potential (50–100 V) occur on a fast time scale in the edge region after biasing in the range of a few fluctuation correlation times (tens of microseconds).

The fast time evolution of floating potential signals has been fitted to the function $V_{fl}(t) = V_{max}\exp(-t/\tau) + V_{min}$, from which the exponential relaxation time τ is deduced. Experimental results show that floating potential signals can be well fitted with characteristic time decay in the range of 10–40 μs. Figure 1 shows the fast decay time and the fitting function of floating potential measured at different plasma radii of the TJ-II plasma edge after switch-off of the biasing for similar plasma conditions ($n_e \approx 0.7 \times 10^{19}$ m^{-3}). Results suggest a decrease of the decay time when moving radially inward inside the plasma.

The influence of plasma density [in the range $(0.4–1) \times 10^{19}$ m^{-3}] on relaxation times has also been investigated in TJ-II. In order to compare with results obtained from the model, the average ion saturation current, measured when switching off the biasing and normalized to its value at the critical point (i.e., when shear flow develops), has been used. Figure 2 shows the behavior of the measured relaxation time at the TJ-II plasma edge ($0.75 < r/a < 0.85$) after switch-off of the biasing as a function of the above-mentioned control parameter as well as the corresponding signals and fits for two different values of the parameter. Results suggest an increase in decay times above the critical value of the parameter (i.e., once edge perpendicular sheared flows are fully developed).

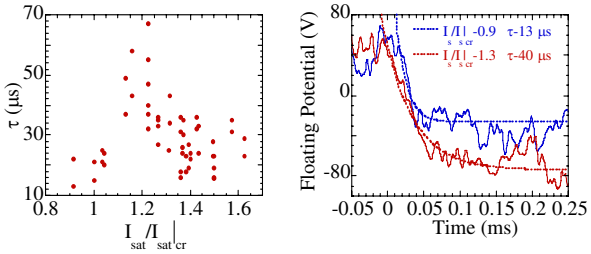

Fig. 2. Left: Decay times of floating potential signals measured in the TJ-II plasma edge ($r/a \sim 0.8$) as a function of local density (i.e., ion saturation current) gradient at the electrode switch-off time. Right: Fitting of floating potential measured in plasmas with different line-average density.

Turbulent damping mechanisms are likely to apply for short time scales, of the order of a few turbulence correlation times (typically $\tau_c \sim 10$ μs); this is consistent with the time decay found experimentally. Momentum losses via atomic physics mechanisms (charge exchange) might also play a role. However, using typical edge plasma parameters, the damping times due to charge exchange are expected to be on the order of hundreds of microseconds, significantly larger than the decay time measured experimentally. Parametric studies of the influence of different plasma regimes (e.g., collisionality, turbulence correlation times, magnetic configuration) on the damping time of poloidal flows and radial electric fields as well as comparative experiments in tokamaks and stellarators [10] are in progress. This result should help to quantify the relative influence of anomalous versus neoclassical mechanisms on damping physics of radial electric fields and poloidal flows in fusion plasmas.

In the mid-1990s, a simple model [11] was proposed to explain the transition from low (L-mode) to high confinement mode (H-mode) [12]. The model consists of coupled envelope equations for the fluctuation intensity and the mean electric field shear. In the model, the transition appears as a second-order phase transition with order parameter the poloidal velocity shear V'_θ. The mechanism for the transition is a flow-shear dynamo instability that amplifies the shear flow through the Reynolds stress term. The amplified sheared flow reduces the turbulence fluctuations through the associated sheared electric field turbulence suppression effect [3, 13]. A later extension of this model [14] predicts two successive transitions. The first is a second-order transition controlled by the poloidal shear flow which leads to a reduction of the turbulence level. The second is a first-order transition controlled by the pressure gradient, which leads to the suppression of turbulence. This second state seems to accurately describe the

H-mode state. The first transition (the second-order one) is essentially the same one given by the initial model and has the characteristic properties of the emergence of the sheared flow layer.

We have used the transition model to compare the predictions of this first transition with the experimental results of the formation of this sheared flow layer, as observed in TJ-II. In order to do so, we normalize all the physical magnitudes to their values at the critical point so that we can write the solutions of the model in terms of measurable quantities. Comparisons between the model and experimental data show that in spite of the simplicity of the model, it captures the qualitative features of the transition near the critical point [15]. Note that the model has no free parameters once the position of the critical point is determined. Of course this comparison does not confirm the exact values of the power dependences, but it shows that they are compatible with the data.

The effective viscosity at the plasma edge can be determined by measuring the decay rate of the perpendicular flow once the driving force has been removed. A biased electrode can produce this driving force externally. Decay-rate times obtained from biasing experiments performed in TJ-II have been used as input to investigate the properties of the damping rate in the framework of a model based on the one previously described, but with the addition of an external drive [16]. For short time scales after switching off the bias potential, the model reproduces the exponential decay of the flow and also shows an increase of decay time close to the critical point (Fig. 3), giving a qualitative description of the change of the decay time obtained experimentally that has been shown in Fig. 2 (left).

In conclusion, the evolution of plasma potential, electric fields, and turbulence has been investigated during edge biasing experiments in the TJ-II stellarator. In particular, it has been found that the plasma potential fast decay time when the external torque is suppressed (bias switched off) is in the range of a few fluctuation correlation times. The experimental results can be explained using a simple second-order phase transition model that reproduces many of the features of the TJ-II experimental data and of the transition near the critical point.

M. A. Pedrosa, C. Hidalgo, B. A. Carreras, C. Silva,[1] and L. García[2]
Laboratorio Nacional de Fusion, Asociación EURATOM-CIEMAT, Madrid, Spain
E-mail: angeles.pedrosa@ciemat.es
[1] Associação EURATOM/IST, Centro de Fusão Nuclear, Lisboa, Portugal
[2] Universidad Carlos III, Madrid, Spain

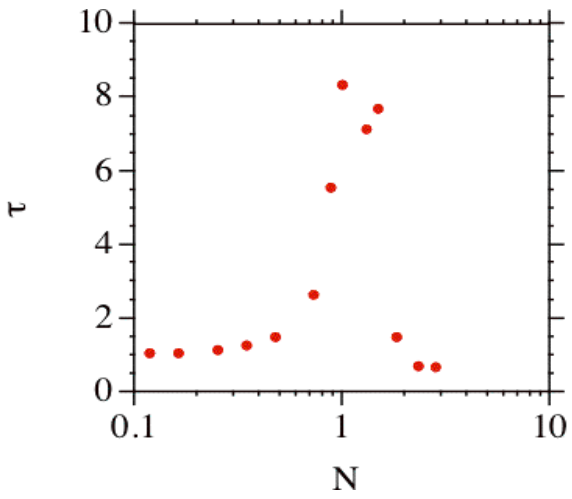

Fig. 3. Decay time obtained by the model as a function of the local average ion saturation current normalized at the corresponding critical point (*N*).

References

[1] K. Burrell, Phys. Plasmas **6** (1999) 4418.
[2] B. A. Carreras, IEEE Trans. Plasma Sci. **25** (1997) 1281.
[3] P. W. Terry, Rev. Mod. Phys. **72** (2000) 109.
[4] K. C. Shaing and E. C. Crume, Phys. Rev. Lett. **63** (1989) 2369.
[5] A. B. Hassam and T. M. Antonsen, Phys. Plasmas **1** (1994) 337.
[6] P. H. Diamond and Y. B. Kim, Phys. Fluids **3** (1991) 1626.
[7] B. A. Carreras et al., Phys. Fluids B **3** (1991) 1438.
[8] C. Silva et al., Czech. J. Phys. **55** (2005) 1589.
[9] M. A. Pedrosa et al., Plasma Phys. Control. Fusion **47** (2005) 777.
[10] M. A. Pedrosa et al., EPS-2007.
[11] P. H. Diamond, Y. M. Liang, B. A. Carreras, and P. W. Terry, Phys. Rev. Lett. **72** (1994) 2565.
[12] F. Wagner, G. Becker, K. Behringer, et al., Phys. Rev. Lett. **49** (1982) 1408.
[13] H. Biglari, P. H. Diamond, and P. W. Terry, Phys. Fluids B **2** (1990) 1.
[14] B. A. Carreras, D. E. Newman, P. H. Diamond, and Y.-M. Liang, Phys. Plasmas **1** (1994) 4014.
[15] B. A. Carreras, L. García et al., Phys. Plasmas **13** (2006) 122509.
[16] B. A. Carreras et al., in preparation.

Electron Bernstein wave heating by OXB-mode conversion at low magnetic field in the WEGA stellarator

One of the most efficient methods of magnetized plasma heating is electron cyclotron resonance heating (ECRH) using microwaves. However, ECRH via ordinary (O-mode) or extraordinary (X-mode) electromagnetic waves is limited by the cutoff density n_{cutoff} and could not be used in an overdense plasma ($n > n_{cutoff}$). In order to overcome this limit, the electrostatic electron Bernstein wave (EBW) [1] can be used. This wave can propagate in the plasma without cutoff limits. However, EBW must be generated via mode conversion from O- or X-waves, which has been demonstrated in several fusion devices [2,3]. In this paper we describe the successful application of a heating scheme applying the mode conversion from O-mode to X-mode and subsequently to EBW (OXB) [4] at low magnetic field in the WEGA [5] stellarator (Max-Planck-Institut für Plasmaphysik, Greifswald).

The mode conversion requires a density gradient with a characteristic normalized density scale length $k_0 L_n$, which is about 10, where $k_0 = 2\pi/\lambda_0$ is the wave number of the incident wave in vacuum, λ_0 is the free space wavelength, $L_n = |n_e/\nabla n_e|$ is the characteristic density scale length at the upper hybrid resonance (UHR) layer, and n_e is the plasma electron density. In our new approach for low-frequency OXB heating, the density profile must be flattened to achieve $k_0 L_n$ of 1–20.

The mode conversion region is situated in the scrape-off plasma outside the separatrix, where the density scale length is typically 10 cm, which results in $k_0 L_n = 5$ for the 2.45-GHz vacuum wavelength ($\lambda_0 = 12.24$ cm). In addition to the technological aspects, the application of OXB at long wavelengths provides a unique opportunity to investigate the mode conversion process; the O-X conversion process can be clearly demonstrated by the radially resolved measurement of the phase and amplitude of the waves involved in the conversion process using high-frequency probes [6]. The EBW absorption process is investigated by temporal modulation of the microwave source and observation of the concomitant oscillations in electron temperature and density.

In the OXB mode conversion process, first an externally launched O-mode is coupled to a slow X-mode (SX) in the region of the O-mode cutoff layer ($n_e = n_{e\_cutoff} = 7.5 \times 10^{16}$ m^{-3}). The SX-mode propagates to the UHR layer, where it is converted into an electrostatic EBW as shown in Fig. 1(c). The EBW propagates into the overdense plasma where it is absorbed in the cyclotron resonance region [7]. This method requires launching the radio frequency (RF) power with O-mode polarization and wave vector $\vec{k}$ under an optimal oblique orientation with respect to the external magnetic field given by the Mjølhus [8] formula. For WEGA the maximum conversion efficiency is reached at an optimal angle $\theta_{opt} = 50°$. Even though the optimal value for θ_{opt} is obtained in the Wentzel-Kramer-Brillouin (WKB) approximation limit, which is not satisfied in WEGA at 2.45 GHz, the OXB conversion process is not fully described by the WKB approximation but requires full-wave calculations [9]. We have developed a finite-difference time-domain (FDTD) full wave code to describe the microwave behavior for WEGA conditions. The code solves Maxwell's equations on a two-dimensional grid in a horizontal plane near the antenna using a cold fluid plasma model. The solution region is bounded with numerical absorbers.

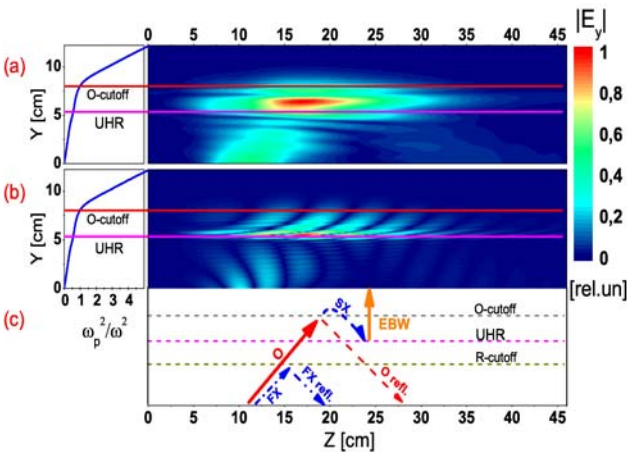

Fig. 1. Full-wave calculation of the OX conversion process. (a) Time averaged and (b) instantaneous *y*-component of the wave ***E*** field distribution. The arrows illustrate the wave propagation in mode conversion processes (c).

Fig. 1(a) shows the calculated time-averaged electric field component $\boldsymbol{E}_y$, while the instantaneous electric field amplitude is shown in Fig. 1(b). Here y and z are the radial and toroidal coordinates in the equatorial plane. The code uses the measured plasma density and the vacuum magnetic field distribution as input data. The heating power source is simulated using the vacuum antenna field pattern.

The O-mode radiation emanating from the microwave source (located at the bottom left of Fig. 1a and b) propagates towards the O-cutoff layer, where it is converted into the SX-mode. The unconverted part of the radiation is reflected. The SX-mode is resonant near the UHR layer, where it is numerically identified by its short wavelength, and is absorbed. This is modeled with a numerical viscosity term. The artificial damping allows the estimation of

the O-SX conversion efficiency by comparing the transmitted heating power with the unconverted power returned to the absorbing boundary. In a real finite-temperature plasma, the SX-wave is converted into a Bernstein wave at the UHR layer.

WEGA is a medium-sized classical $l = 2$, $m = 5$ stellarator, with major radius $R \approx 72$ cm and maximum plasma radius a ≈ 11 cm. The plasma is generated by up to 26 kW of 2.45-GHz ECRH power in a steady-state discharge, typically for 30 s in hydrogen, helium and argon. A heating power modulation with frequency up to 12.5 kHz is also possible. To obtain the resonant conditions in plasma, the magnetic field strength is around 0.087 T. However, pulsed operation is also possible with magnetic field strength more than 0.5 T. For ECRH and diagnostics, 100 ports are available. The largest port diameter is in the equatorial plane and has a diameter of 92 mm. The heating antenna could be installed in this port; however, it is still limited by the distance to the last closed flux surface (LCFS). A waveguide with 83 mm Ø and two slots in the side wall (10 cm length and 64° angular width) showed the best heating performance. The ECRH power is launched into two lobes with corresponding $\theta = \pm 42°$. This is the closest to the ideal $\theta_{opt} = 50°$ that could be achieved within the space limitations. The high-frequency emission is linearly polarized in the horizontal plane. Table 1 shows the improvement of the numerically calculated OX conversion efficiency $\tau_{O\text{-}SX}$ and improved plasma performance using the double-slot antenna in comparison to that of an open waveguide of the same diameter.

Table 1. O-X mode conversion efficiency and plasma parameters for different heating antennas.

	Open waveguide	Double slot
$\tau_{O\text{-}SX}$ [8]	6.7%	20%
$\tau_{O\text{-}SX}$ full wave	5.2%	25%
n/n_{e_cutoff}	1.5 (hollow profile)	12 (peaked profile)
T_e (eV)	<6	<20

The presence of Bernstein waves, the final step of the OXB conversion, is shown in heating power modulation experiments. The power is modulated at 12 kHz on a time scale faster than the typical ~1-ms confinement time in WEGA. The perturbation amplitude represents the power deposition, while the slope in the phase of perturbation shows the direction of energy propagation away from the power deposition region. Both are measured with Langmuir probes, which are positioned in the equatorial plane separated by a toroidal angle of 144° from the heating antenna position.

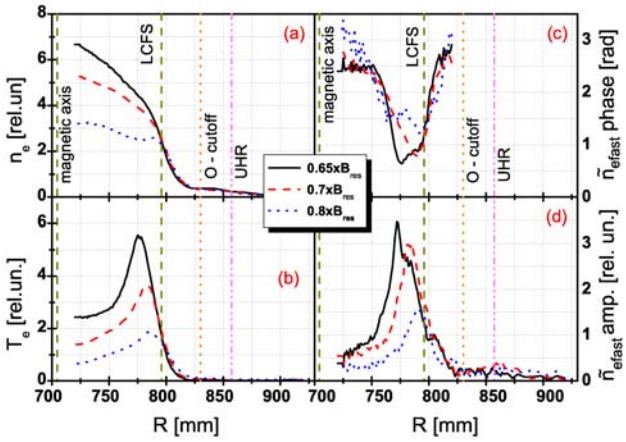

Fig. 2. Plasma parameters measured by Langmuir probes during power modulation experiments: (a) relative electron density profile, (b) relative thermal electron temperature profile, (c) relative phase, and (d) amplitude of the perturbation of the fast electron. Heating power is 3 kW.

The density, thermal electron temperature and fraction of fast electrons are determined from Langmuir probe measurements using a two-temperature model [10]. A set of four probes is used at fixed biases of –90 V, –25 V, 0 V, and 20 V. The probes are separated from each other by 5 mm in the poloidal direction and are radially scanned across the plasma. Even though the probe characteristic is estimated by only four points, and thus the absolute accuracy of the plasma parameters is less than that from the full-characteristic-swept single probe, the relative T_e and n_e profiles are reproduced quite well. Absolute calibration is not necessary for modulation experiments. The absolute values of typically $T_e \sim 12$ eV and $n_e \sim 10^{18}$ m^{-3} were measured by a slowly sweeping single-pin probe and a central line-of-sight microwave interferometer. Figure 2 shows results of the plasma perturbation measurements for a range of magnetic fields, where $B_{res} = 87$ mT corresponds to the electron cyclotron resonant field at 2.45 GHz. The perturbation of density of fast electrons [Fig. 2(d)] is largest and strongly localized inside the LCFS in the overdense plasma region. This indicates the power deposition location. No significant perturbation is found near the UHR layer; no notable power deposition is observed in this region. The phase [Fig. 2(c)] shows the propagation of the perturbation away from the deposition region, which is explained by hot electron transport.

The results of EBW propagation simulations with OXB conversion efficiency and ray-tracing calculations [11] show good agreement of power deposition profiles with the profiles measured during power modulation experiments. In Fig. 3 the power deposition profiles calculated for a range of magnetic fields are presented. The measured

density, temperature, magnetic field profiles, and antenna emission pattern were used in these calculations.

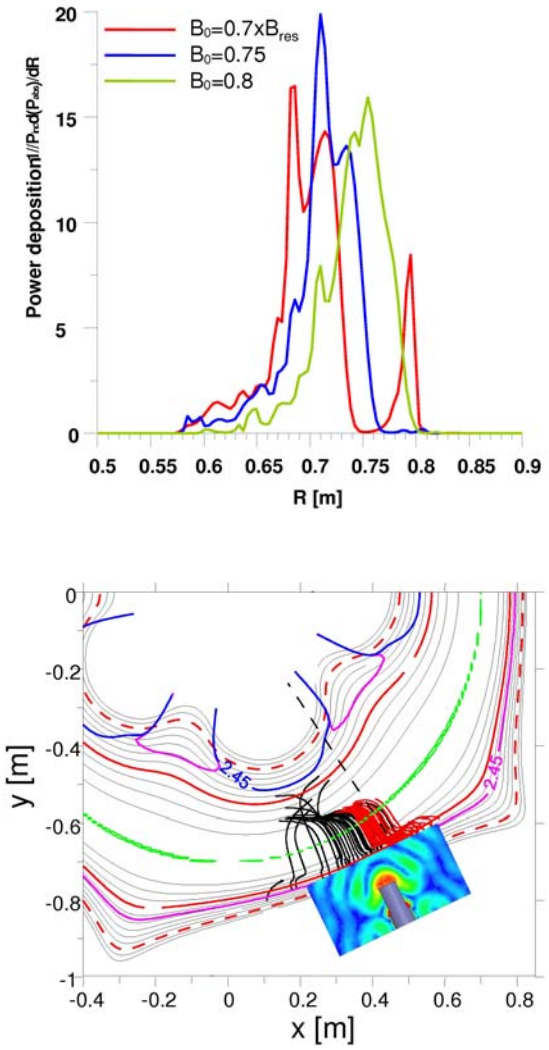

Fig. 3. Power deposition calculated using OXB conversion efficiency (top) and the ray-tracing simulation code result (bottom).

The magnetic field dependence of the power deposition location (Figs. 2 and 3) provides clear evidence of local resonant EBW heating of the overdense plasma. The absorption is concluded to be strongly Doppler-shifted [9] to lower frequencies, peaking at $B = 0.65\ B_{res}$, where maximum line integrated density is also observed. This indicates a resonant interaction of the EBW, with a large refractive index component in the direction parallel to the vacuum magnetic field, with high parallel velocity suprathermal electrons.

Highly overdense plasma production has been achieved using OXB heating in the WEGA stellarator at low magnetic field. The conversion from O-wave to X-wave was demonstrated by direct measurements of the wave field [6] in the conversion region. The results were supported by full wave calculations. The propagation and resonant absorption of Bernstein waves were measured in fast power modulation experiments. It was shown that the Bernstein waves are absorbed by suprathermal electrons with a strongly Doppler shifted cyclotron resonance, which was confirmed by ray tracing calculations. Full wave simulations show that a much higher OXB conversion efficiency can be obtained if the heating antenna is designed to emit the HF wave with optimal elliptical polarization and a narrow $\hat{k}$ spectrum [6]. The experiments demonstrate that OXB-mode conversion heating is not restricted to high magnetic field fusion devices but is also applicable in low magnetic field plasma experiments for basic plasma physics research and industrial applications.

Y. Y. Podoba, H. P. Laqua, G. B. Warr, M. Schubert, M. Otte, S. Marsen, F. Wagner, and D. Andruczyk
Max-Planck-Institut für Plasmaphysik, EURATOM Association
D-17491 Greifswald, Germany
E-mail: yuriy.Podoba@ipp.mpg.de

E. Holzhauer
Institut für Plasmaforschung Univ. Stuttgart
D-70569 Stuttgart, Germany

J. Preinhaelter, J. Urban
EURATOM/IPP.CR Association, Institute of Plasma Physics
182 21 Prague, Czech Republic

References

[1] I. I. Bernstein, Phys. Rev. **109**, 10 (1958).

[2] A. Mueck et al., 32nd EPS Conference on Plasma Phys., Tarragona, ECA Vol. 29C, P-4.110 (2005).

[3] H. P. Laqua, V. Erckmann, H. J. Hartfuss, and H. Laqua, Phys. Rev. Lett. **78**, 3467 (1997).

[4] J. Preinhaelter and V. Kopeck´y, Plasma Phys. **10**, 1 (1973).

[5] M. Otte et. al., "Five Years of WEGA operation at IPP Greifswald," *Stellarator News*, Issue 106, p. 4.

[6] Y. Y.Podoba et. al., "Direct Observation of Electron Bernstein Wave Heating by OXB-Mode Conversion at Low Magnetic Field in the WEGA Stellarator," Phys. Rev. Lett. (accepted for publication).

[7] M. Bornatici, Plasma Phys. Control. Fusion **28** (4), 629–645 (1986).

[8] E. Mjølhus, Plasma Phys. **31**, 7 (1984).

[9] S. Nakajima and H. Abe, Phys. Lett. A **124** (4,5), 295 (1987).

[10] P. C. Stangeby, Plasma Phys. Control. Fusion **37**, 1031–1037 (1995).

[11] J. Preinhaelter, J. Urban, et al., "Simulation of EBW Heating in WEGA," 17th Topical Conference on Radio Frequency Power in Plasmas, May 7–9, 2007, AIP Proc. (submitted).